Buckling and post-buckling behavior of beams with internal flexible joints resting on elastic foundation modeling buried pipelines

Vasileios E. Melissianos*
School of Civil Engineering – Institute of Steel Structures
National Technical University of Athens
9 Iroon Polytechneiou str., Zografou Campus
GR-15780, Athens, Greece
email: melissia@mail.ntua.gr
tel: +302107722553

Charis J. Gantes
School of Civil Engineering – Institute of Steel Structures
National Technical University of Athens
9 Iroon Polytechneiou str., Zografou Campus
GR-15780, Athens, Greece
email: chgantes@central.ntua.gr
tel: +302107723440

*Corresponding author

KEYWORDS: Winkler beam, internal flexible joints, buckling analysis, buckling mode cross-over, geometrically nonlinear analysis, imperfection sensitivity

ABSTRACT

The buckling and post-buckling behavior of axially loaded Winkler beams with flexible internal hinges is addressed, aiming to provide a background for the investigation of upheaval buckling of buried pipelines equipped with flexible joints for their protection against activation of reverse seismic faults. In order to acquire qualitative understanding of the interaction between the hinge stiffness and the soil stiffness for different cases, the beams under investigation are considered as either simply-supported or clamped. At first, elastic critical buckling loads and corresponding eigenmodes are numerically obtained using linearized buckling analysis, and eigenmode cross-over is investigated considering soil and hinge rotational stiffness. Geometrically nonlinear analyses with imperfections (GNIA) are then performed, indicating for most cases descending post-buckling paths, thus unstable post-buckling behavior, with the exception of cases of very soft soil. The sensitivity of the response to initial imperfection shape and magnitude is also addressed, to identify their impact on the post-buckling behavior. Beam buckling behavior is moreover examined by considering the beam being surrounded by soil exhibiting different stiffness in the upward and the downward direction. The results are compared to the case of a continuous beam, in order to highlight the impact of internal hinges on the beam overall buckling behavior.

1. INTRODUCTION

The so-called Winkler model of a beam resting on elastic foundation is a commonly applied engineering approach in various problems involving interaction between a structural member and the surrounding soil, due to its reliability and computational simplicity and efficiency. Applications of this model can be found in different areas of soil – structure interaction, such as foundation engineering, buried structures and railway tracks. Soil is considered as a single layer that can be represented by a series of closely spaced and mutually independent transverse springs with proportional resistance to deflection. Different aspects regarding the overall buckling behavior of continuous beams resting on elastic foundation can be found in the literature [1]-[5]. Timoshenko and Gere [6] showed the impact of soil stiffness on the critical eigenmode shape of axially loaded simply-supported Winkler beams, demonstrating that variation of soil stiffness may lead to eigenmode cross-over. Wu and Zhong [7] implemented the energy method to analytically investigate the buckling of elastically supported beams of finite length under compression for different end conditions, identifying eigenmode transition and then carried out post-buckling analysis of perfect beams and using post-buckling curvature to examine beam stability. Rao and Neetha [8] developed a detailed analytical methodology to estimate the elastic foundation stiffness that corresponds to the first transition of the critical eigenmode, using free vibrations. Buckling and post-buckling behavior of beams resting on elastic foundation was also investigated by Kounadis et al. [9], who derived analytical expressions of the post-buckling equilibrium path for a 1-DOF model. Song and Li [10] focused on thermal buckling and post-buckling of pinned – fixed beams on elastic foundation; they introduced a so called “shooting method” to analytically solve the complex boundary condition problem and also adopted the energy method to describe post-buckling behavior considering buckling temperature. Li and Batra [11] presented equations for buckling and post-buckling behavior of laterally supported simply-supported and clamped beams. The major conclusions of this study included the insignificant impact of the nonlinear foundation parameter on the buckling load temperature and the post-buckling deformation. Aristizabal-Ochoa [12] introduced

a methodology to estimate the critical buckling load of axially loaded columns resting on Winkler foundation with generalized end conditions.

The aforementioned studies deal with beams of finite length. However, elongated structures, such as railway tracks and pipelines, are usually modeled as infinite beams. In such case, buckling localization emerges as an important issue. Localization of the buckling pattern depends among others on the applied axial force and the soil stiffness. Research on this topic is extensive and several researchers have presented rigorous analytical studies, trying to deal with the significant nonlinearity of the problem through advanced mathematical tools, among which prominent is the work by Hunt and Wadee (e.g. [13-[16]).

In cases of buried steel pipelines crossing tectonic faults, flexible joints between pipeline parts have been proposed as mitigating measures against the consequences of possible fault activation [17]. Such joints are effective in protecting the pipelines from the two most common failure modes encountered in such cases, namely local buckling due to high compressive strains and girth weld fracture due to high compressive strains, by absorbing deformation through relative rotation of adjacent pipeline parts, which then remain virtually undeformed. However, in case of reverse faults high compressive axial forces may develop along the pipeline, and the reduction of overall stiffness induced by the flexible joints may lead to a third possible failure mode, which is flexural buckling, also known as upheaval buckling, as the pipeline may then deform outside the trench.

A Winkler beam with flexible internal hinges constitutes an appropriate model to investigate the potential of upheaval buckling when the pipeline is subjected to combined bending and compression due to reverse faulting [18],[19]. An internal hinge modifies the beam global stiffness and consequently affects the corresponding buckling and post-buckling behavior. The extent of this effect depends on the relative pipeline – joint – soil stiffness and must be taken into account in case such mitigating measures are proposed. The buckling behavior of an axially loaded, clamped beam without lateral support and with two internal hinges was presented by Wang [20]. The author applied an analytical approach to maximize the critical buckling load

through the optimization of hinges' location. Later, Wang [21] extended the formerly developed model by introducing a single elastic support to strengthen the hinge location. The critical buckling load of an elastic beam with various end conditions was maximized by optimizing the hinge location considering the elastic restraint stiffness. Later, Wang [22] presented a more detailed model of a beam resting on elastic foundation to address the optimum hinge location for maximizing the critical buckling load and recently he presented an analytical study on the buckling of an infinite beam resting on elastic foundation with one or more internal hinges subjected to compressive force [23].

The topics of buckling behavior and eigenmode cross-over of continuous beams that rest on elastic Winkler foundation have been discussed in depth by previous researchers, as summarized above. However, the pertinent work regarding internally hinged beams is limited. Aiming at addressing this issue, in the present study the effect of hinge rotational stiffness on eigenmode cross-over with respect to soil stiffness is first quantified by means of numerical linear buckling analysis. Furthermore, the beam post-buckling behavior is not adequately addressed in the existing literature. Hence, this study then focuses on the numerical investigation of the beam post-buckling behavior through geometrically nonlinear imperfection analysis. Simply-supported and clamped boundary conditions are considered, with the second being representative of the deformed shape assumed by buried pipelines that are subjected to fault activation. Two cases of internal hinges are analyzed: an internal hinge located in the beam middle and two internal hinges equally spaced along the beam. The internal hinges are assumed to be equipped with elastic rotational springs, while relative translations of the two beam parts at each hinge are restrained, to represent a hinged flexible joint.

As mentioned above, the beam buckling behavior is first studied through linearized buckling analysis [24], and the results are directly compared to the corresponding ones in cases of continuous beams [25]. Parametric studies highlight the effect of soil stiffness, hinge rotational stiffness and beam boundary conditions on critical buckling loads and eigenmode shapes. Geometrically nonlinear analyses are then carried out, providing useful conclusions regarding

the post-buckling behavior, imperfection sensitivity and the effect of soil restraint on ultimate loads. Additionally, the effect on beam response of different upward and downward springs with different stiffness is investigated compared to elastic soil in terms of ultimate loads. Research results can be significant for hazardous structures such as pipelines, as well as other major facilities such as railway tracks, as the design assumptions and safety factors to be considered are highly affected.

2. ANALYSIS MODEL

In order to investigate the overall buckling response of an Euler-Bernoulli beam with internal hinges resting on elastic or elastoplastic foundation, an appropriate numerical approach has been adopted. This approach is considered as suitable for dealing with this problem from a structural design rather than engineering mechanics point of view, as it can in future be readily extended to issues that are commonly encountered in practice, such as non-straight pipeline route, inhomogeneous soil conditions, varying axial force distribution along the pipeline accompanied by bending moments, etc.

In case of buried pipelines subjected to fault rupture, the source of the applied action on the structure, namely the fault location, is well defined. If the fault is activated, the pipeline is forced to follow the ground motion and to deform on the two sides of the fault in an s-shaped pattern extending to two so-called anchor points, one on each fault side, beyond which the developing stress-state is nearly negligible. If the fault is reverse, significant axial compression develops in the pipeline, with a maximum value at the fault and gradually diminishing towards the anchor points due to soil friction. Aiming at addressing this problem in a simplified, conservative manner, the adopted numerical model is that of an elastic Winkler beam of length L, defined by the anchor points, and flexural rigidity EI, subjected to axial compressive force P. It is also noted that the adopted model of a finite beam for the simplified pipeline modeling is sufficient regarding also the issue of buckling localization, taking into account that the location of the source of the applied action is well defined, while the anchor points represent the assumed

boundary conditions. To that effect, either hinged or clamped boundary conditions are considered at the two ends, even though for long struts actual boundary conditions are less significant as the deflections and their derivatives all tend to zero near the boundaries. Furthermore, the problem is treated as static, given that the dynamic effects of fault movement are considered by pertinent codes as negligible ([26]-[27]).

The beam longitudinal displacement is denoted by x and the transverse displacement by $y(x)$. Beams rest on Winkler foundation that exhibits stiffness k_s, which is normalized via the expression:

$$K_s = k_s L^4 / EI \quad (1)$$

and ranges from a minimum value K_s = 180 to a maximum value K_s = 20000. Three characteristic soil stiffness values are selected, namely K_s = 180, K_s = 10000 and K_s = 20000, which correspond to the critical eigenmode shape of the continuous beam being the first symmetrical, the first antisymmetrical and the second symmetrical, respectively. These soil stiffness values are selected based on the fact that soil stiffness increase leads to eigenmode cross-over for the continuous beam among the three above mentioned types of modes [25]. Furthermore, the selected soil stiffness values are reasonable assumptions for the soil stiffness of upward soil springs in buried pipeline analysis. For example, the value K_s = 10000 corresponds to a small diameter, shallowly buried pipe in dense backfill sand, while K_s = 180 to a large diameter, deeply buried pipe backfilled with loose sand. Estimation of soil springs' stiffness for buried pipelines is carried out using the suggestions of pertinent codes and provisions (e.g. ALA [26], EC8 [27], ASCE [28]) or expressions found in the literature [29] depending on the backfill material properties. According to these sources, the soil material laws are nonlinear, idealized in practice for the design of buried pipelines against faulting as elastic – perfectly plastic. In the present work linear soil springs have been assumed, while in section 4.5 the effect of soil nonlinearity has been investigated, considering different soil stiffness in the upwards and downwards directions. In the numerical model, Winkler soil is modeled with transverse springs that connect beam nodes to fixed "ground" nodes and exhibit stiffness only in

the axial direction corresponding to their undeformed state. It is noted that in the literature nonlinear soil properties with softening effects have also been considered, for example by Yang and Bradford [30], who showed that the softening soil parameter plays an important role in localization phenomena and the post-buckling response of infinite beams.

The internal hinge of the beam is equipped with an elastic rotational spring of stiffness k_r and practically replaces the beam flexural rigidity. The corresponding rotational stiffness is normalized via the expression:

$$K_r = k_r \, / \left(EI \, / \, L \right) \tag{2}$$

In the subsequent analyses the internal hinge rotational stiffness is appointed with five characteristic values, i.e. K_r = 0, 2, 5, 10 and 45. The value K_r = 0 represents the case of a "pure" internal hinge without stiffness, while stiffness K_r = 45 was found to be sufficiently high to almost restore the beam flexural continuity. It is noted that the selected range of rotational stiffness conforms to the corresponding stiffness of commercially available hinged flexible joints. Thus, the rotational stiffness of the internal hinge can be selected by the design engineer in order to monitor the strain reduction of the structure, achieved by the use of the joints. The stiffness of such joints increases as the pipe diameter increases, while the maximum rotational capacity decreases. Thus, the selected range, apart from the maximum value that is related to beam continuity restoration, is realistic for flexible joints in pipeline applications that are expected to undergo large rotations due to faulting.

The beam analysis models are depicted in Figure 1 through Figure 4 by considering two cases of internal hinges: an internal hinge located at the beam middle or two internal hinges equally spaced along the beam. In particular, the simply-supported beam with one internal hinge is shown in Figure 1, the simply-supported beam with two internal hinges in Figure 2, the clamped beam with one internal hinge in Figure 3 and the clamped beam with two internal hinges in Figure 4.

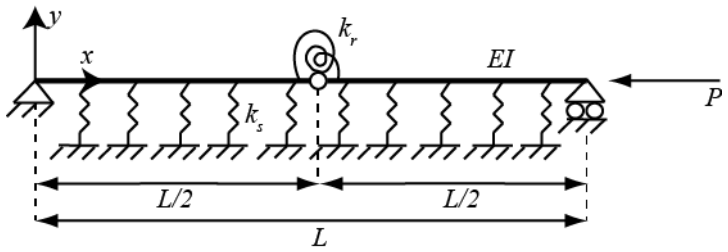

Figure 1: Simply-supported beam resting on foundation with one internal hinge

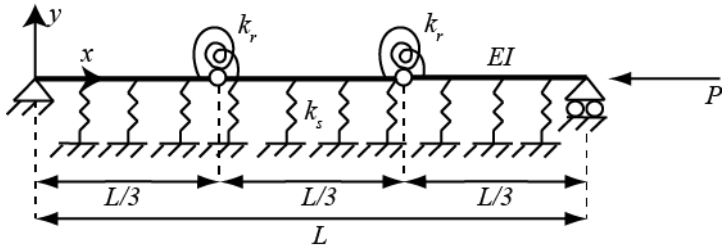

Figure 2: Simply-supported beam resting on foundation with two internal hinges

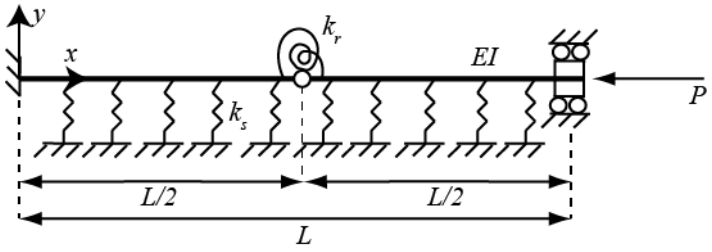

Figure 3: Clamped beam resting on foundation with one internal hinge

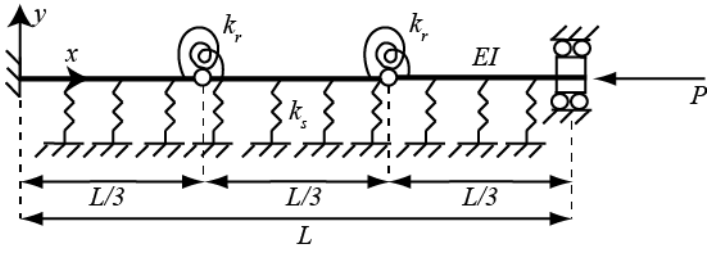

Figure 4: Clamped beam resting on foundation with two internal hinges

3. LINEAR BUCKLING ANALYSIS

Linear Buckling Analysis (LBA) is carried out using the commercial FEM software ADINA [31] according to the so-called “classical” buckling formulation described by Bathe [32]. According to this formulation eigenmodes and buckling loads are obtained from the equation:

$$
\begin{aligned}
&{}^{t_1}_{0}\mathbf{K}\varphi_i = \gamma_i\left({}^{t_1}_{0}\mathbf{K} - {}^{t_1}_{0}\mathbf{K}_g\right)\varphi_i \Rightarrow \left(1-\frac{1}{\lambda_i}\right)\left({}^{t_1}_{0}\mathbf{K} - {}^{t_1}_{0}\mathbf{K}_g\right)\varphi_i \Rightarrow {}^{t_1}_{0}\mathbf{K}_g\varphi_i = \frac{1}{\lambda_i}\left({}^{t_1}_{0}\mathbf{K}_g - {}^{t_1}_{0}\mathbf{K}\right)\varphi_i \Rightarrow \\
&\left(\left({}^{t_1}_{0}\mathbf{K} - {}^{t_1}_{0}\mathbf{K}_g\right) + \lambda_i\,{}^{t_1}_{0}\mathbf{K}_g\right)\varphi_i = 0 \Rightarrow \left({}^{t_1}_{0}\mathbf{K}_0 + {}^{t_1}_{0}\mathbf{K}_u + \lambda_i\,{}^{t_1}_{0}\mathbf{K}_g\right)\varphi_i = 0
\end{aligned}
\tag{3}
$$

where ${}^{t_0}_{0}\mathbf{K}$ and ${}^{t_1}_{0}\mathbf{K}$ are the stiffness matrices of the structure at time t_0 and t_1 respectively, t_0 is the time at the beginning of the analysis, t_1 is equal to $t_0 + \Delta t$, where Δt is a time increment. Then, φ_i is the i-th eigenmode and γ_i is a function of the eigenvalue λ_i with $\gamma_i = 1 - 1/\lambda_i$. The formulation of Eq. (3) leads to the evaluation of the classical buckling load when t_0 corresponds to the unloaded situation and t_1 to a loaded structure with sufficiently small applied reference loads ${}^{t_1}\mathbf{R}$ [33]. The critical buckling load is determined from the critical load factor λ_1 via the expression:

$$
\mathbf{R}_{cr,i} = \lambda_i\,{}^{t_1}\mathbf{R} \tag{4}
$$

Verification of the “classical” method of buckling analysis in ADINA has been provided by many researchers (e.g. [34]-[36]).

3.1 SIMPLY-SUPPORTED BEAM

3.1.1 Beam with one internal hinge

The simply-supported beam of Figure 1 with an internal hinge located in the middle is considered. The critical buckling load of the beam with one internal hinge (Figure 1) with reference to soil stiffness and hinge rotational stiffness is illustrated in Figure 5. The critical buckling load (P_{cr}) is plotted on the vertical axis and normalized with respect to the Euler load ($P_{E,ss}$) of the continuous simply-supported beam without elastic support, while the normalized soil stiffness (K_s) is plotted on the horizontal axis. The buckling load of the continuous beam is also presented for comparison reasons. A first observation is that the increase of the rotational stiffness leads to the gradual restoration of the beam continuity. The buckling load curve for small K_r values is a smooth curve without notable turning points, in contrast to the continuous beam, where three evident turning points indicate the eigenmode cross-overs.

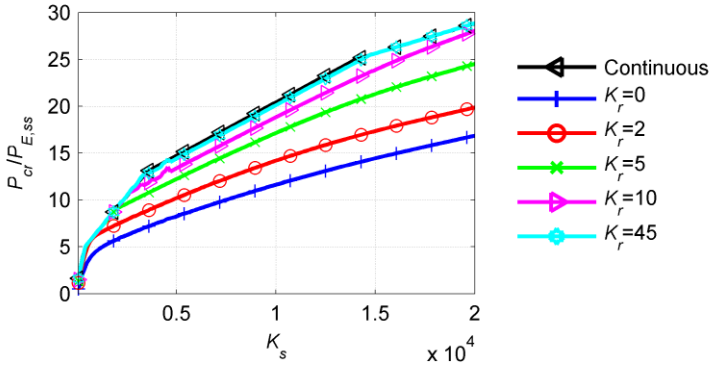

Figure 5: Normalized critical buckling load of simply-supported beam with one internal hinge with respect to soil stiffness for varying hinge rotational stiffness

Results extracted from Figure 5 regarding the eigenmode cross-over are confirmed by Figure 6 that shows the critical eigenmodes. The critical eigenmodes for rotational stiffness ranging from K_r = 0 to K_r = 10 are all symmetric and the corresponding shape reveals that eigenmode cross-over is absent as soil stiffness increases. The internal hinge weakens the beam at the middle and its location dominates the eigenmode shape. On the other hand, for K_r = 45, two eigenmode cross-overs take place. The critical eigenmode is symmetric with single curvature for K_s = 180, becomes symmetric with two intermediate inflection points for K_s = 10000, and finally it turns into antisymmetric for K_s = 20000. Eigenmode cross-over is thus encountered, defined as the transition of eigenmode shapes with respect to soil stiffness.

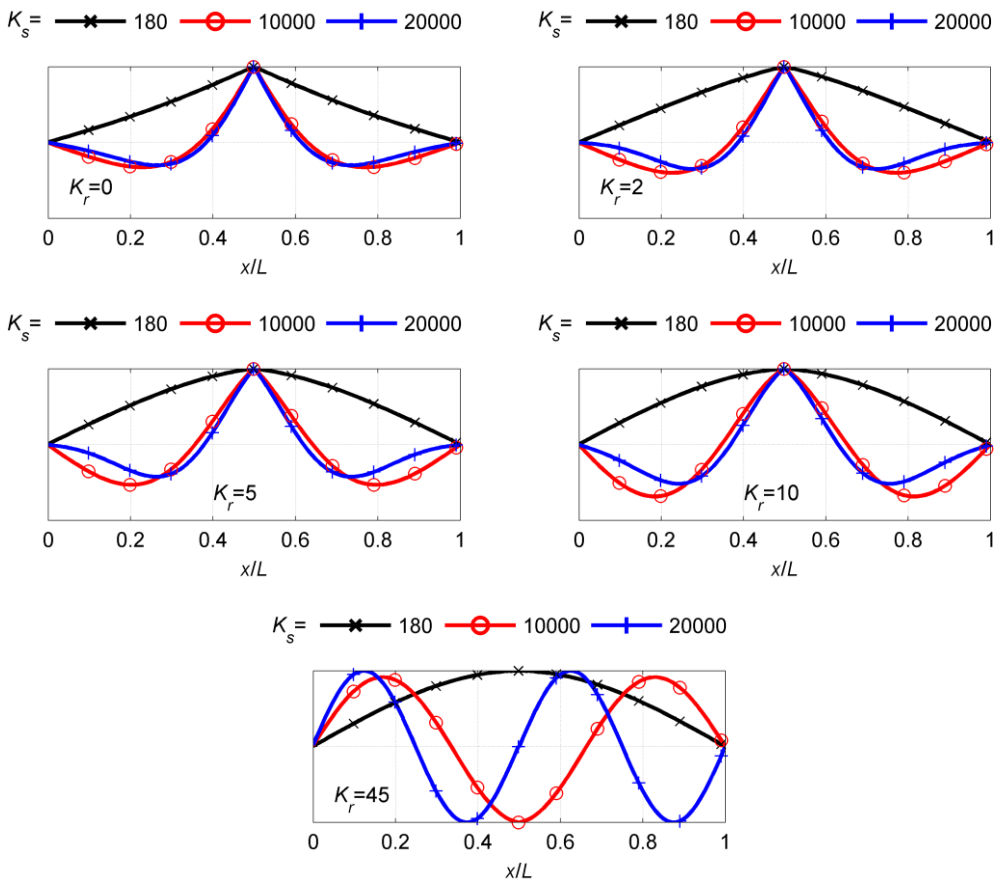

Figure 6: Critical eigenmodes of simply-supported beam with one internal hinge for varying hinge rotational stiffness

3.1.2 Beam with two internal hinges

The critical buckling load of the beam with two internal hinges (Figure 2) is presented in Figure 7, where again the critical buckling load (P_{cr}) is plotted on the vertical axis, normalized with respect to the Euler load of the continuous beam without elastic support ($P_{cr,ss}$), and the normalized soil stiffness (K_s) is plotted on the horizontal axis. Similar qualitative conclusions are extracted as in the case of one hinge, with the load P_{cr} increasing with soil stiffness as well as with joint stiffness. For small K_r values the buckling load curve indicates no eigenmode cross-over, and the resulting buckling loads are smaller than the ones of the beam with one hinge. Increasing rotational stiffness reveals the gradual restoration of the beam continuity and consequently the increase of buckling load.

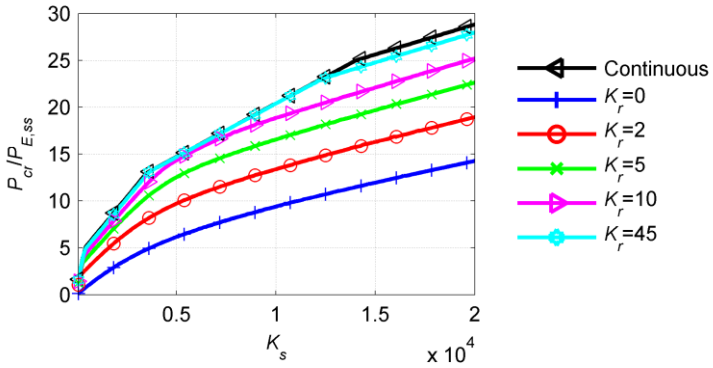

Figure 7: Normalized critical buckling load of simply-supported beam with two internal hinges with respect to soil stiffness for varying hinge rotational stiffness

The conclusions derived from Figure 7 regarding the eigenmode cross-over are confirmed by Figure 8, where the critical eigenmodes are illustrated. The symmetrically located hinges highly affect the critical eigenmode shape for small hinge rotational stiffness and thus in Figure 8 all eigenmodes are antisymmetric. As K_r increases to values of 5 and 10, eigenmode cross-over is detected. The critical eigenmode is symmetric for low soil stiffness and is similar to the first symmetric eigenmode of the continuous beam. Increasing soil stiffness leads to cross-over. Antisymmetric eigenmode shapes are dominated by hinge locations. Finally, the maximum rotational stiffness restores the beam continuity and similar results as in the beam with one hinge are observed (see Figure 6).

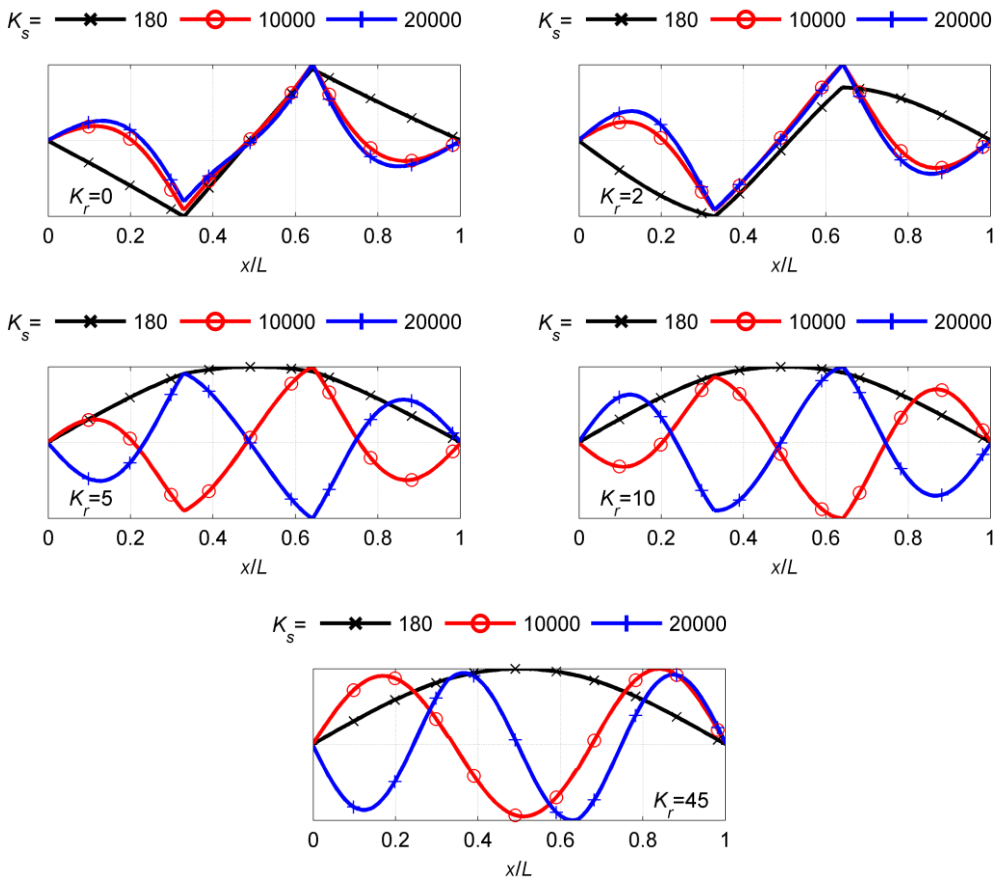

Figure 8: Critical eigenmodes of simply-supported beam with two internal hinges for varying hinge rotational stiffness

3.1.3 Critical buckling loads of simply-supported beams

The comparison between critical buckling loads of continuous and internally hinged simply-supported beams is necessary to highlight the consequences of internal hinges in terms of reducing beam global stiffness. This direct comparison is illustrated in Figure 9 for two characteristic rotational stiffness values, namely K_r = 0 that represents the case of a pure hinge and K_r = 10. The case of a “pure” hinge (K_r = 0) leads to a dramatic decrease of the critical buckling load. At the same time, the difference between the continuous beam (C), the beam with one internal hinge (1H) and the beam with two internal hinges (2H) rises as soil stiffness increases. On the contrary, stiffness K_r = 10 that corresponds to partial beam continuity restoration leads to the reduction of the difference between the buckling loads. For the case of K_s = 10000 the difference between beams C and 1H is minimized. It is noted that the critical

buckling load reduction due to the integration of internal hinges in a beam resting on foundation under compressive axial force was also reported for the case of an infinite beam by Wang [23].

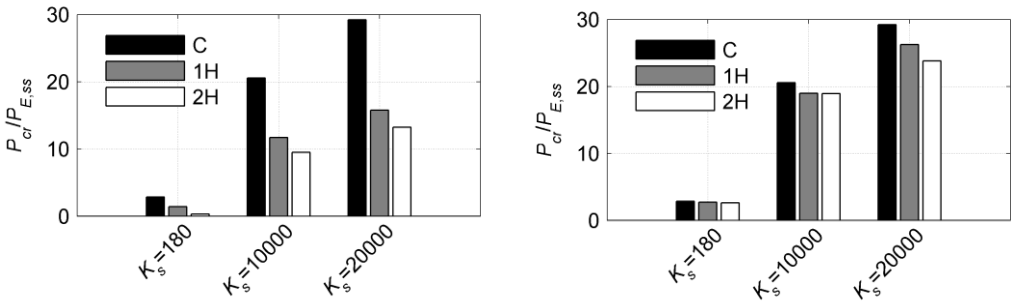

(a) (b)

Figure 9: Critical buckling loads of simply-supported beams for (a) K_r = 0 and (b) K_r = 10

3.2 CLAMPED BEAM

3.2.1 Beam with one internal hinge

The critical buckling load evolution of the clamped beam with one internal hinge (Figure 3) with respect to soil stiffness is illustrated in Figure 10. The load P_{cr} is presented on the vertical axis and is normalized with respect to the Euler load of the clamped continuous beam without elastic support ($P_{E,cl}$). P_{cr} increases as soil stiffness increases. The increase of rotational stiffness restores the beam continuity and yields to buckling load gradual increase, similarly to previous cases.

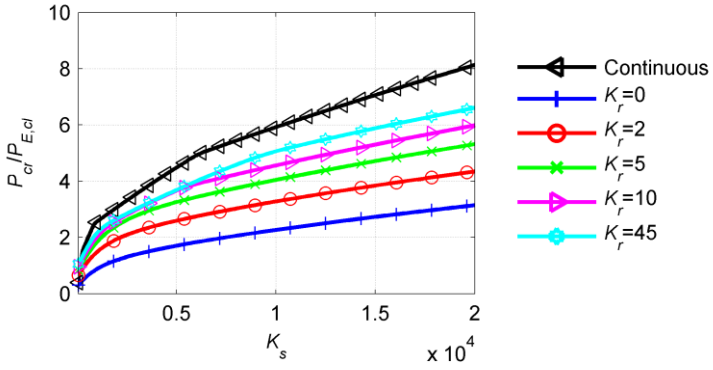

Figure 10: Normalized critical buckling load of clamped beam with one internal hinge with respect to soil stiffness for varying hinge rotational stiffness

The eigenmode cross-over is examined in Figure 11, where the critical eigenmodes are illustrated. The centrally located internal hinge dominates the symmetric critical eigenmode shapes for K_r values ranging from 0 to 5. As the critical eigenmode shape is transformed consecutively from symmetric to antisymmetric, one eigenmode cross-over for K_r = 10 and three cross-overs for K_r = 45 are observed.

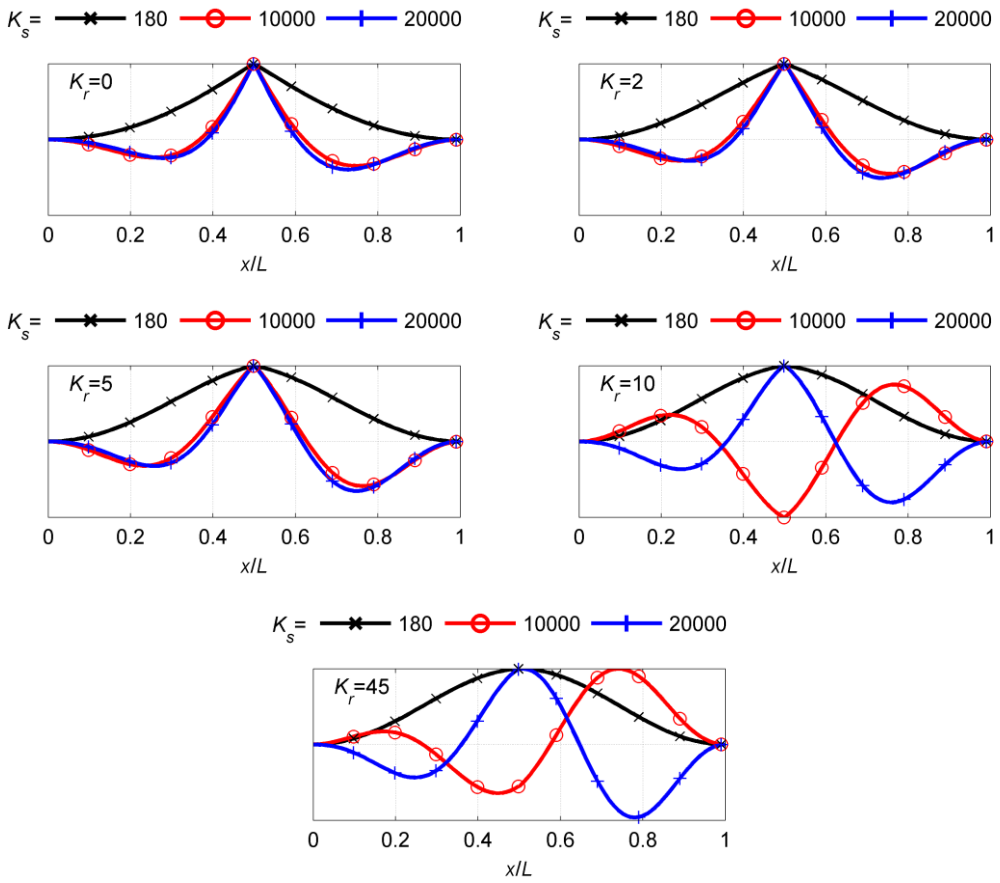

Figure 11: Critical eigenmodes of clamped beam with one internal hinge for varying hinge rotational stiffness

3.2.2 Beam with two internal hinges

The critical buckling load P_{cr} of the clamped beam with two internal hinges (Figure 4) is illustrated in Figure 12, normalized with respect to the Euler load of the clamped continuous beam without elastic support ($P_{E,cl}$) and presented versus the normalized soil stiffness. The load P_{cr} increases as soil stiffness increases, following the same pattern with all previous cases. The equally spaced internal hinges alter the beam stiffness depending also on their rotational

stiffness. The buckling load curve for small K_r indicates that eigenmode crossover does not occur. This outcome is confirmed by considering the eigenmode shapes presented in Figure 13 for varying rotational stiffness.

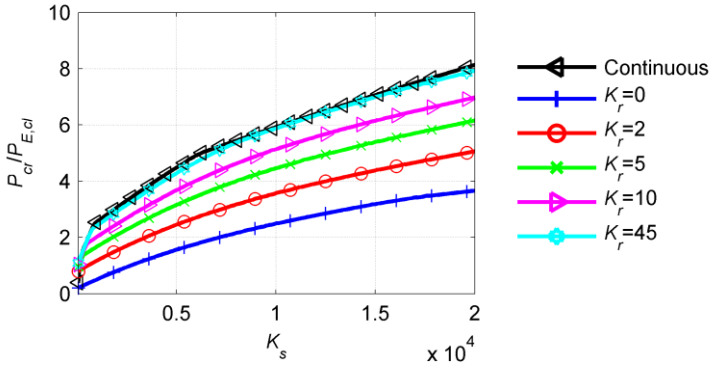

Figure 12: Normalized critical buckling load of clamped beam with two internal hinges with respect to soil stiffness for variable hinge rotational stiffness

The symmetrically introduced hinges dominate the critical eigenmode shapes. It becomes clear from Figure 13 that for small rotational stiffness all eigenmodes are antisymmetric, even though increasing soil stiffness slightly modifies the shape. As K_r increases to values of 5 and 10, eigenmode cross-over occurs, and the symmetric shape is transformed to antisymmetric for soil stiffness greater than K_s = 10000. Finally, the maximum rotational stiffness reestablishes beam continuity and similar results to the clamped beam with one internal hinge can be extracted (see Figure 11).

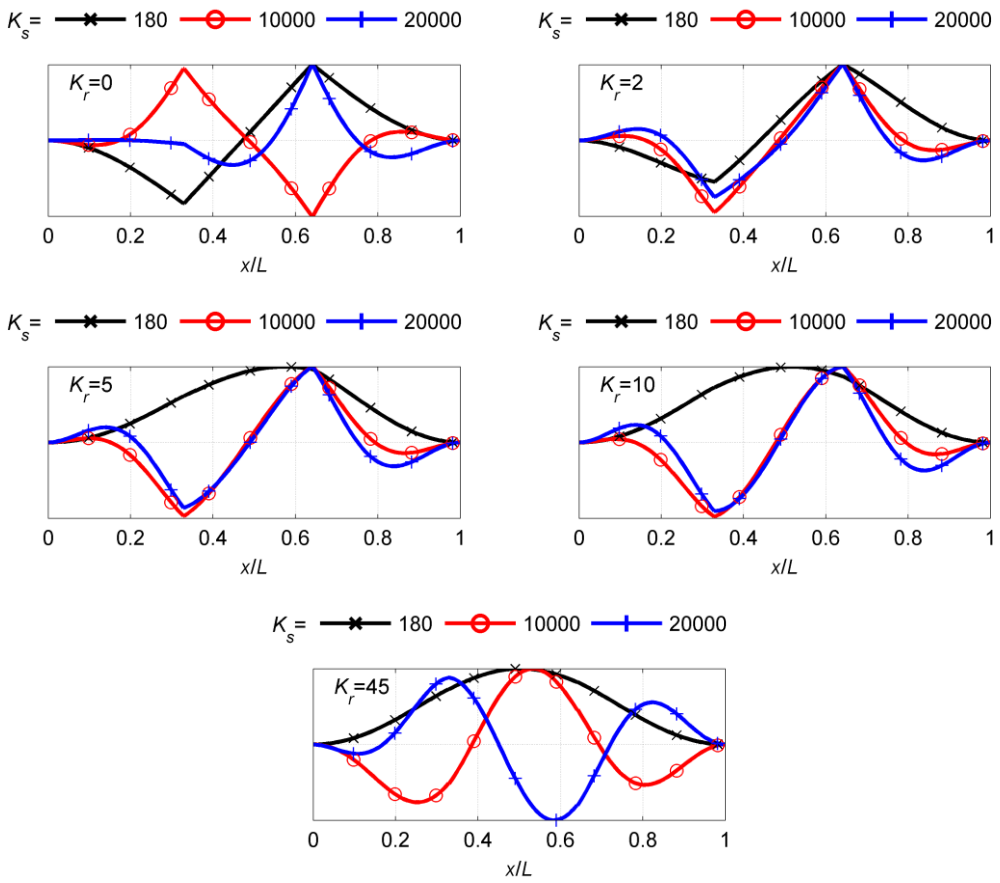

Figure 13: Critical eigenmodes of clamped beam with two internal hinges for variable hinge rotational stiffness

3.2.3 Critical buckling loads of clamped beams

The introduction of either one or two internal hinges has a direct impact on the clamped beam's buckling behavior also. The critical buckling loads of the continuous beam (C), the beam with one hinge (1H) and the beam with two hinges (2H) are compared in order to quantify this influence. The normalized buckling loads are presented in Figure 14 for two characteristic rotational stiffness values, namely K_r = 0 and K_r = 10. A pure hinge (K_r = 0) leads to a decrease of buckling load levels compared to the continuous beam. The difference in critical buckling loads between the continuous beam, the beam with one internal hinge and the beam with two internal hinges rises as soil stiffness increases. The difference between the buckling loads is relatively reduced for the case of K_r = 10 that corresponds to partial beam continuity restoration. A significant difference exists between the simply-supported and the clamped beam. The

clamped boundary conditions affect the buckling loads of 1H and 2H beams, as the double hinged beam has higher buckling load than the single hinged beam in the majority of the cases presented in Figure 14. This is attributed to the fact that the hinges are now closer to the clamped supports, and thus contribute less to beam stiffness reduction.

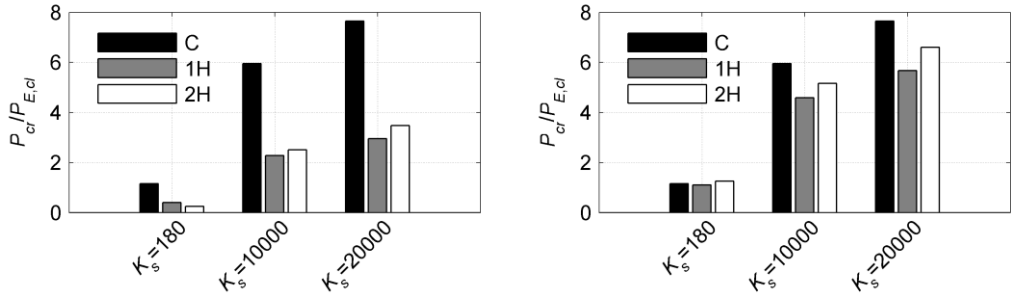

Figure 14: Critical buckling loads of clamped beams for (a) K_r = 0 and (b) K_r = 10

4. GEOMETRICALLY NONLINEAR ANALYSIS

4.1 ANALYSIS METHODOLOGY AND IMPERFECTIONS

The assessment of post-buckling behavior of buckling – sensitive structures necessitates the implementation of advanced numerical techniques [37]. In the present study nonlinear numerical analyses are carried out using the commercial FEM software ADINA [31] that incorporates the "arc-length" type algorithm for tracing the post-buckling equilibrium path [38]. Results obtained from ADINA using nonlinear solution algorithms have been compared against experimental ones in the literature (e.g. [39]-[42]) for a wide range of problems, including among others local and global buckling of steel structures.

The presence of unavoidable initial imperfections may significantly affect the response of buckling – sensitive structures and must be taken into account for their analysis and design. Considering that actual imperfections are unknown during design, a commonly adopted approach regarding imperfection shape is to use a linear combination of buckling modes (e.g. [37], [43]-[44]). According to this approach, in the present study linear combinations of the first four eigenmodes are adopted as initial imperfections and incorporated in the geometrically

nonlinear analysis. The shape of eigenmodes is extracted from Linearized Buckling Analysis of section 3. Linear combinations of eigenmode shapes that are used as initial imperfections in the subsequent nonlinear analysis are listed in Table 1, aiming at quantifying the effects of imperfections in the structural response and detecting all possible imperfection sensitivities. Buckling and hence post-buckling behavior of beams resting on elastic foundation is dominated by soil stiffness, as a potential increase may lead to eigenmode cross-over. Consequently, various initial imperfection shapes are considered, given that the shape of the first symmetric eigenmode may not be adequate to identify any potential imperfection sensitivity. The imperfections under consideration are initially normalized so that their amplitude equals $L/500$, as a typical, rather small value employed in practice for steel members according to code provisions.

Table 1: Imperfection combinations for geometrically nonlinear analysis

Imperfection	Linear combination
I	mode 1 + mode 2 + mode 3 + mode 4
II	mode 1 + mode 2 - mode 3 + mode 4
III	mode 1 + mode 2 + mode 3 - mode 4
IV	mode 1 + mode 2 - mode 3 - mode 4

It is important to point out that the choice of buckling modes as imperfection patterns is not unique and may not cover all eventualities, as in many cases it has been found to lead to lower compliance to experimental results than other shapes of initial imperfections (e.g. [37]). Additionally, Schneider and colleagues [45],[46] have shown that considering different imperfection patterns may be important, depending also on the imperfection magnitude, while amplitude-dependent imperfection patterns cannot be determined with confidence. Hence, GNIA results should be interpreted accordingly and imperfection size must also be investigated, as will be shown in the following.

In Geometrically Nonlinear Imperfection Analysis (GNIA), equilibrium equations are formulated in the deformed configuration of the structure that is allowed to differ significantly from the undeformed one. This type of analysis is necessary for investigating buckling and, mainly, post-

buckling structural behavior, through the equilibrium path relating the applied action with the deformation corresponding to a characteristic degree of freedom of the structure. In the present investigation the position along the beam with maximum transverse displacement (y_{max}) at the analysis end is selected for all equilibrium paths. Hence, the transverse displacement normalized with respect to the beam length (y_{max}/L) is plotted on the horizontal axis, while the applied axial load normalized with respect to the critical buckling load of the continuous beam resting on soil ($P/P_{cr,cs}$), either simply-supported [1] or clamped [12], is plotted on the vertical axis, while the dashed line represents the critical buckling load obtained from LBA. The beam deformed shape at the analysis end is displayed and compared to the shapes of initial imperfections and eigenmodes, leading to conclusions.

A double – parameter problem with soil stiffness and hinge rotational stiffness acting as the two dominating parameters is formulated. For the sake of brevity, indicative values of the parameters are selected and the associated numerical results are presented. The linearized buckling analysis results (section 3) and the relationships between soil stiffness and critical buckling loads with reference to hinge rotational stiffness (Figure 5, Figure 7, Figure 10 and Figure 12) indicate that the rotational stiffness value K_r = 5 leads to beam continuity restoration by almost 50%, thus nonlinear analysis results are presented for this case.

4.2 SIMPLY-SUPPORTED BEAM

The simply-supported beam with one internal hinge resting on elastic foundation (Figure 1) is at first numerically investigated and indicative results for soil stiffness K_s = 180 are shown. The first four eigenmodes are presented in Figure 15(a) and the initial imperfection shapes according to Table 1 are illustrated in Figure 15(b). The nonlinear analysis results are presented in terms of equilibrium paths in Figure 16(a) and beam deformed shape at the end of the analysis in Figure 16(a), for all different cases of initial imperfections. It is observed that all equilibrium paths practically coincide and have descending post-buckling behavior. Such unstable post-buckling behavior is crucial from design point of view, indicates high imperfection sensitivity and should

be addressed accordingly through appropriate safety factors, as structural safety cannot rely on post-buckling strength. It is also noted that the ultimate loads are close to the critical buckling load that is displayed with the dashed line. The beam deformed shape is also not affected by imperfections shapes, but is dominated by the critical eigenmode shape, as illustrated in Figure 16(b). Numerical results for soil stiffness K_s = 10000 and K_s = 20000 lead to similar conclusions. It should be noted that nonlinear analysis carried out for soil stiffness much lower than the minimum value considered here, i.e. K_s = 180, showed that the buckling overall response is stable indicating that in such case the response is similar to the simply-supported beam without lateral support.

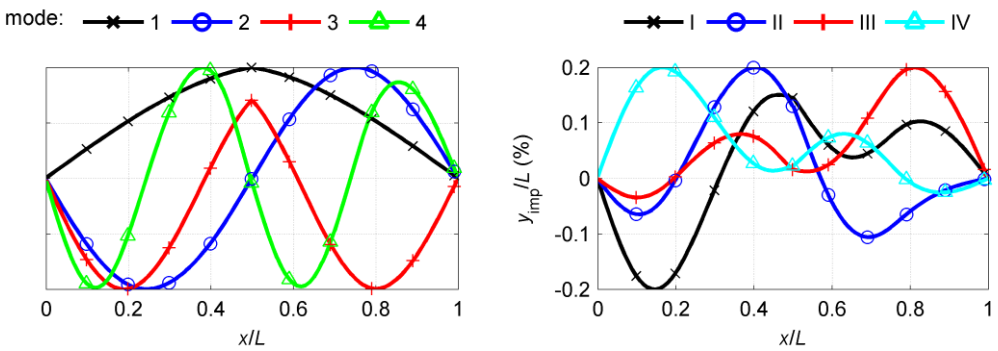

(a) (b)

Figure 15: (a) Eigenmode shapes and (b) imperfection shapes considered in GNIA for simply-supported beam with one internal hinge for K_s = 180 and hinge rotational stiffness K_r = 5

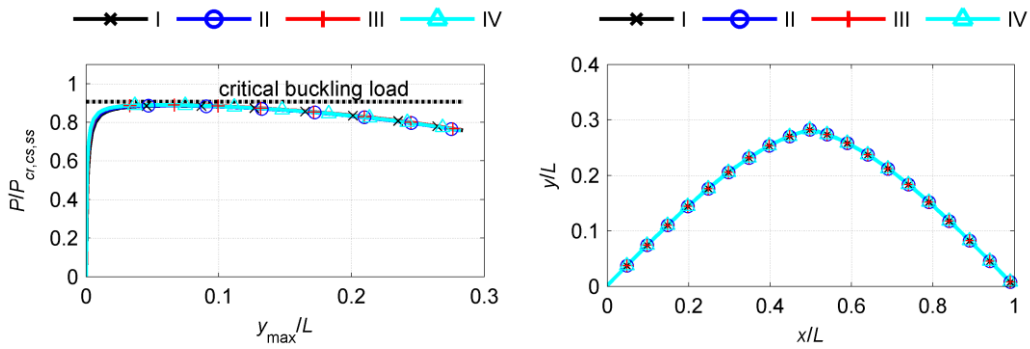

(a) (b)

Figure 16: (a) Equilibrium paths and (b) beam deformed shapes from GNIA of simply-supported beam with one internal hinge for K_s = 180 and hinge rotational stiffness K_r = 5

The increase of soil stiffness leads to eigenmode cross-over with reference to the hinge rotational stiffness. It is therefore essential to examine the beam behavior and especially the beam deformed shape at the end of nonlinear analysis by considering soil stiffness values being close enough to the value that corresponds to the transition point $K_s \approx 533$, characterized by the critical eigenmode being symmetrical before and antisymmetrical after this point. Thus, the simply-supported beam is considered to rest on soil with $K_s = 526$ (before the transition) or $K_s = 540$ (after the transition), with the critical buckling load ratio of the two cases being equal to 0.99. The numerical results (considering the first linear combination of the eigenmodes for the imperfection shape) are presented in terms of the equilibrium path and the beam deformed shape at the end of the analysis in Figure 17(a) and Figure 17(b), respectively. It is observed that the equilibrium paths coincide as the soil stiffness values considered are very close, while the beam deformed shapes are affected by both critical eigenmode shapes, but not to the same extent. Thus, the deformed shape for $K_s = 526$ (before the transition) is closer to symmetrical, having no intersection points with the horizontal axis, while the deformed shape for $K_s = 540$ (after the transition) has an intersection with the horizontal axis, and it is closer to antisymmetrical.

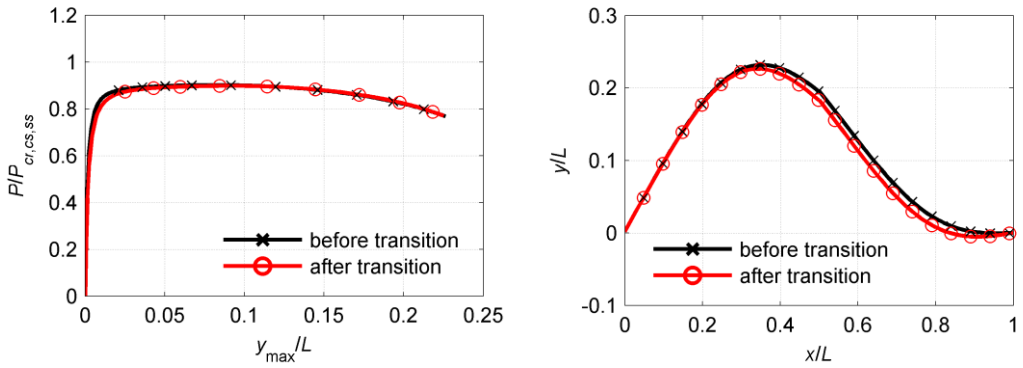

(a) (b)

Figure 17: (a) Equilibrium paths and (b) beam deformed shapes from GNIA of simply-supported beam with one internal hinge for $K_r = 5$ before ($K_s = 526$) and after ($K_s = 540$) the transition point

Next, the simply-supported beam with two internal hinges resting on elastic foundation (Figure 2) is investigated through nonlinear analysis. The first four eigenmodes are illustrated in Figure

18(a) and the imperfection shapes considered in GNIA in Figure 18(b). The analysis results for soil stiffness K_s = 180 are depicted in Figure 19. The equilibrium path is highly nonlinear and the beam post-buckling behavior is unstable, as clearly indicated by the ultimate load and the subsequent descending equilibrium path. Moreover, compared to the beam with one internal hinge, in case of the beam with two internal hinges, the difference of the ultimate load from the critical buckling load obtained from LBA is higher. Then, the beam deformed shape is highly affected by the antisymmetric critical eigenmode, due to the presence of two equally spaced internal hinges, as presented in Figure 19(b). Increasing soil stiffness to K_s = 10000 and K_s = 20000 yields similar results to the beam with one internal hinge regarding the post-buckling behavior, i.e. it is unstable as the equilibrium part is descending after reaching the ultimate load.

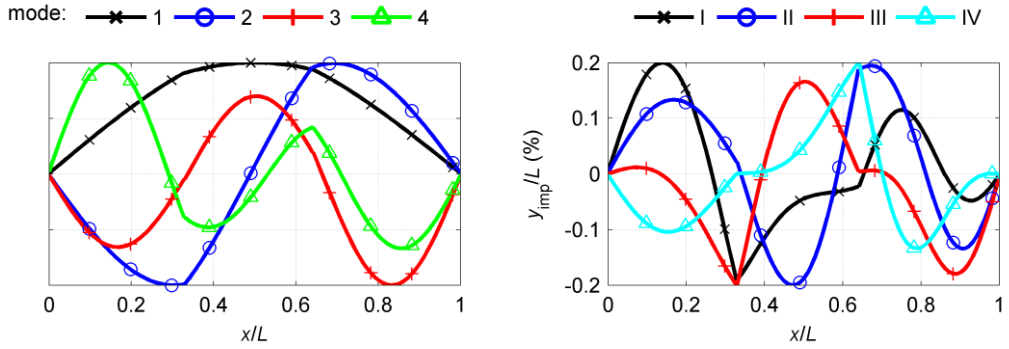

(a) (b)

Figure 18: (a) Eigenmode shapes and (b) imperfection shapes considered in GNIA of simply-supported beam with two internal hinges for K_s = 180 and hinge rotational stiffness K_r = 5

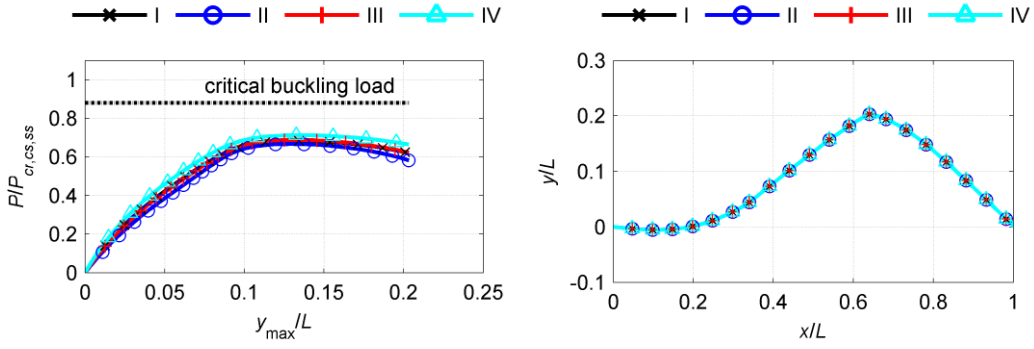

(a) (b)

Figure 19: (a) Equilibrium path and (b) beam deformed shape from GNIA of simply-supported beam with two internal hinges for K_s = 180 and hinge rotational stiffness K_r = 5

The comparison of normalized ultimate loads of a simply-supported continuous beam (C), a beam with an internal hinge (1H) and a beam with two internal hinges (2H) is illustrated in Figure 20. A crucial conclusion is that increasing soil stiffness leads to ultimate load increase in correspondence to critical buckling loads. The internal hinges reduce the ultimate loads with reference to the continuous beam, even though the load levels do not vary significantly among the 1H and the 2H cases. However, the ultimate loads difference grows as soil stiffness increases and the interaction of soil and rotational stiffness emerges in terms of altering the beam post-buckling response.

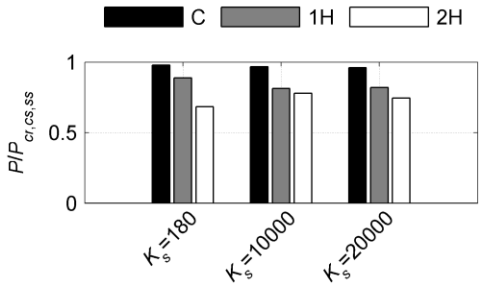

Figure 20: Ultimate loads comparison of simply-supported beams (continuous (C), with one internal hinge (1H) and with two internal hinges (2H)) with hinge rotational stiffness K_r = 5

4.3 CLAMPED BEAM

Next, the buckling and post-buckling behavior of the clamped beam with an internal hinge resting on elastic foundation (Figure 3) is numerically investigated. The eigenmode shapes obtained from LBA (section 3.2.1) and the imperfection shapes considered in GNIA are illustrated in Figure 21(a) and Figure 21(b), respectively, for K_s = 180. The equilibrium path is shown in Figure 22(a), where the primary observation is that the post-buckling behavior is stable due to the low soil stiffness and similar to that of a clamped beam without elastic support (i.e. the elastic beam has post-buckling strength). In order to further substantiate this finding, parametric studies carried out showed that for the case of clamped beam with one internal

hinge, the post-buckling path is unstable for soil stiffness up to K_s approximately equal to 300, for the considered hinge rotational stiffness K_r = 5. The beam deformed shape at the end of the analysis is independent from the imperfections shape and mainly affected by the critical eigenmode shape, as presented in Figure 22(b). On the contrary, numerical results for soil stiffness K_s = 10000 and K_s = 20000 in terms of the equilibrium paths are presented in Figure 23(a) and Figure 23(b), respectively, indicating unstable post-buckling behavior.

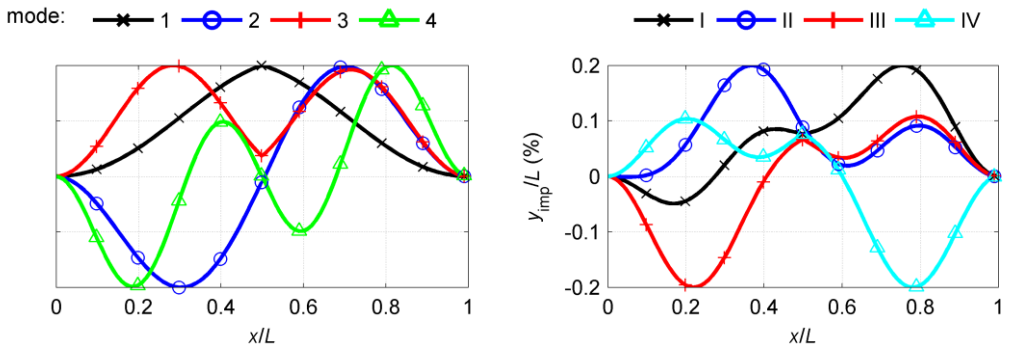

(a) (b)

Figure 21: (a) Eigenmode shapes and (b) imperfection shapes considered in GNIA of clamped beam with one internal hinge for K_s = 180 and hinge rotational stiffness K_r = 5

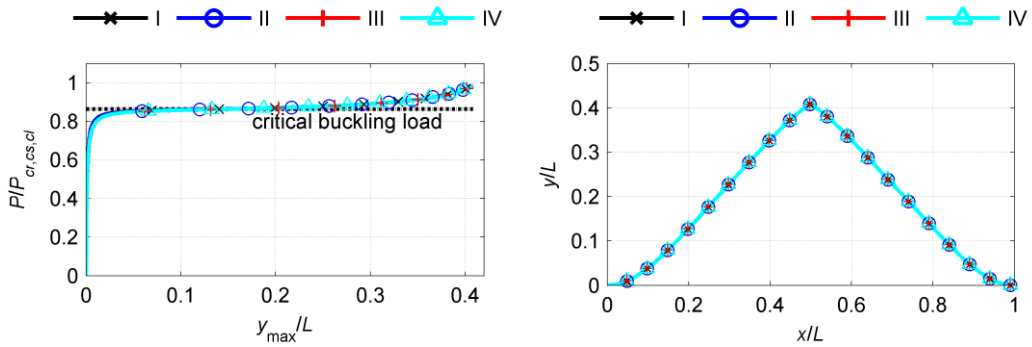

(a) (b)

Figure 22: (a) Equilibrium paths and (b) beam deformed shapes from GNIA of clamped beam with one internal hinge for K_s = 180 and hinge rotational stiffness K_r = 5

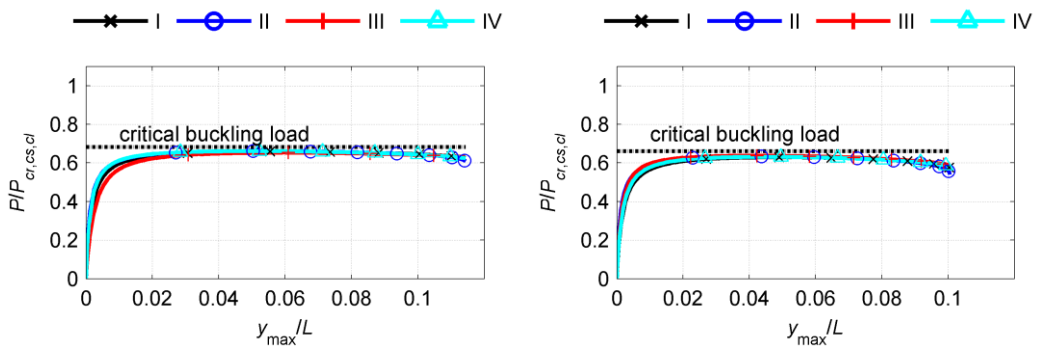

(a) (b)

Figure 23: Equilibrium paths from GNIA of clamped beam with one internal hinge for (a) K_s = 10000 and (b) K_s = 20000 and hinge rotational stiffness K_r = 5

Next, the clamped beam with two equally-spaced internal hinges resting on elastic foundation (Figure 4) is examined. The eigenmode shapes of the beam obtained from LBA (section 3.2.2) and results for soil stiffness K_s = 180 are illustrated in Figure 24(a) and the imperfection shapes in Figure 24(b). The beam equilibrium path for low soil stiffness K_s = 180 is ascending and marginally exceeds the critical buckling load. This stable post-buckling behavior is attributed to the very low soil stiffness that does not restrict the beam enough and consequently its behavior is like the beam without lateral support. Additionally, the comparison of the buckling behavior of the simply-supported and the clamped beam for the same low soil stiffness (K_s = 180) reveals that in case of fixed end conditions (clamped beam) the boundaries contribute to the stability of the beam. Thus, the beam response is similar to that of a continuous clamped beam without elastic support and of a clamped beam with one internal hinge resting on foundation with K_s = 180 (Figure 22). This finding has been further examined through parametric studies, which revealed that for the case of clamped beam with two internal hinges, the post-buckling path is unstable for soil stiffness roughly up to K_s = 325, for the considered hinge rotational stiffness K_r = 5. The beam deformed shapes are then depicted in Figure 25(b) and are dominated by the critical eigenmode shape, while geometrical imperfections do not alter the deformed shapes. On the other hand, the beam post-buckling behavior for K_s = 10000 and K_s = 20000 is reported to

be unstable (Figure 26). Initial imperfections do not affect the buckling behavior in all previous cases.

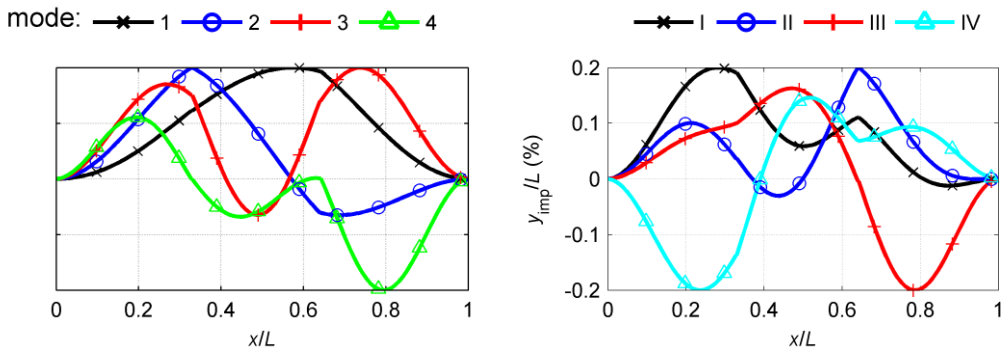

(a) (b)

Figure 24: (a) Eigenmode shapes and (b) imperfection shapes considered in GNIA of clamped with two internal hinges beam for K_s = 180 and hinge rotational stiffness K_r = 5

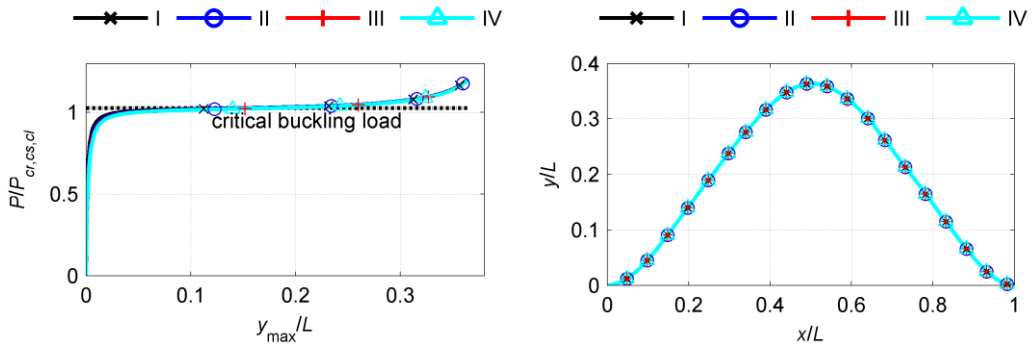

(a) (b)

Figure 25: (a) Equilibrium paths and (b) beam deformed shapes from GNIA of clamped beam with two internal hinges for K_s = 180 and hinge rotational stiffness K_r = 5

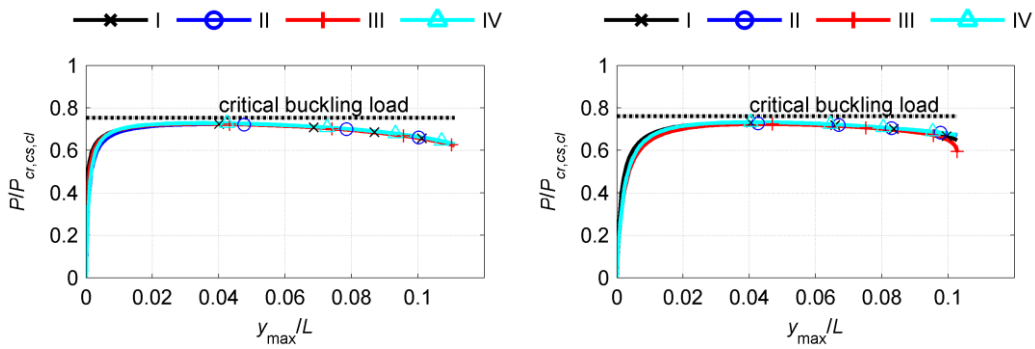

(a) (b)

Figure 26: Equilibrium paths from GNIA of clamped beam with two internal hinges for (a) K_s = 10000 and (b) K_s = 20000 and hinge rotational stiffness K_r = 5

The integration of internal hinges in a clamped beam resting on elastic foundation affects the buckling and post-buckling overall response. The ultimate loads obtained from GNIAs are evaluated to quantify the effects of hinges with reference to the continuous beam. The ultimate loads are compared in Figure 27, where the ultimate loads of a continuous beam (C), a beam with an internal hinge (1H) and a beam with two internal hinges (2H) are presented with respect to soil stiffness K_s = 10000 and K_s = 20000. As already noted, the post-buckling behavior of a clamped beam with one or two internal hinges for K_s = 180 is stable, thus there is no ultimate load, and consequently this soil stiffness is excluded from the comparison. A first observation is that the presence of hinges reduces the loads, while the difference between C and 1H/2H cases increases in terms of loads, as soil stiffness increases. However, the 2H case ultimate load is higher or marginally equal to the 1H for all cases of soil stiffness under investigation. This conclusion is related with the location of the two hinges that are far from the beam center and thus their impact on global stiffness is reduced in contrast with the case of a simply-supported beam (Figure 20).

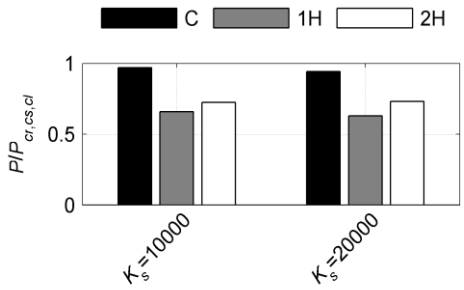

Figure 27: Ultimate loads comparison of clamped beams (continuous (C), with one internal hinge (1H) and with two internal hinges (2H)) with rotational stiffness K_r = 5

4.4 IMPERFECTION MAGNITUDE SENSITIVITY

The ultimate load of a structure with unstable post-buckling behavior is usually sensitive to the size of initial geometric imperfections that are considered in the nonlinear analysis. Regarding

the beam resting on elastic foundation, either simply-supported or clamped with one or two internal hinges, it has been shown in sections 4.2 and 4.3 that, for the very small size of initial imperfection considered there, the shape of the imperfection neither modifies significantly the post-buckling behavior, nor affects the ultimate load. It is then of considerable practical significance to investigate the effect of the imperfection magnitude. The imperfection magnitude in sections 4.2 and 4.3 was considered equal to $L/500$, which is a lower value than those assumed in practice as proposed by pertinent structural codes for structural members (mainly columns and beams). Purpose of that choice was to establish that the post-buckling behavior of such beams is unstable, even for very small imperfections and to confirm that, in such case, the ultimate load is practically coincident with the linear buckling load.

However, regarding buried pipelines, due to constructional reasons and the inherent non-flatness of the trench bottom, the expected initial geometrical imperfections are expected to be much higher than $L/500$. In order to quantify these considerations, the effect of the initial imperfections magnitude is investigated by considering the clamped beam with two internal hinges (Figure 4), considering this simplified structural model being a reasonable assumption for buried pipelines crossing a fault. Four values of imperfection magnitudes are considered, namely $L/500$, $L/100$, $L/50$ and $L/10$.

At first, to identify the effect of imperfection magnitude, only the first linear combination of eigenmodes (Table 1) is adopted as imperfection shape and the corresponding analysis results are presented in terms of equilibrium paths in Figure 28 (a) for soil stiffness $K_s = 180$, where it is shown that the size of initial imperfections modifies the equilibrium path, but the overall buckling response remains stable, even though the linear part of the response is minimized. Then, the equilibrium paths for $K_s = 20000$ are illustrated in Figure 28(b), where the primary important observation is that the increase of initial imperfection size leads to a significant decrease of the ultimate load.

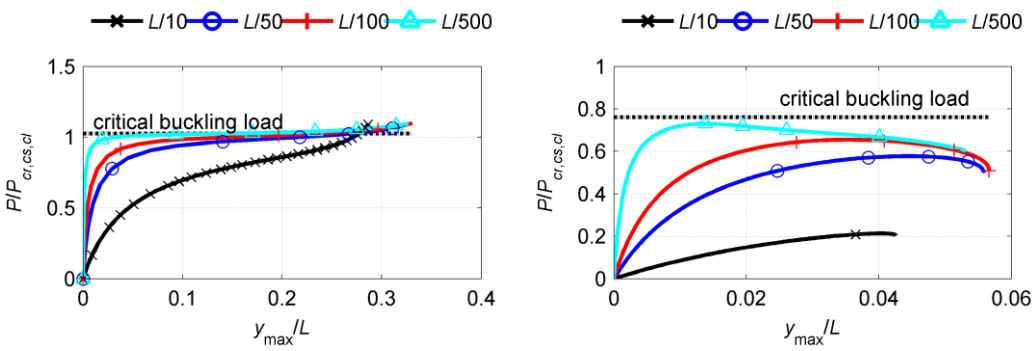

Figure 28: Equilibrium paths for varying imperfection magnitude of clamped beam with two internal hinges for (a) K_s = 180 and (b) K_s = 20000 and hinge rotational stiffness K_r = 5

Then, in order to investigate the interaction between the imperfection shape and magnitude in terms of affecting the ultimate load and the post-buckling behavior of the beam, all imperfection shapes after Table 1 are considered and the equilibrium paths for K_s = 20000 are shown in Figure 29 for imperfection magnitudes L/50 and L/100. It is observed that the increase of imperfection magnitude increases the effect of imperfection shape in terms of altering the ultimate load. Moreover, it has been shown in Figure 26(b) that the buckling and post-buckling response of the clamped beam with two internal hinges is not affected when relatively low imperfection magnitude is considered, namely L/500. Then, the beam deformed shape at the ultimate load is presented in Figure 30 for varying imperfection magnitude and all considered imperfection shapes (Table 1). It is observed that for increased imperfection magnitude the different shapes of initial imperfection lead to modified beam deformed shapes at the ultimate load level in terms of magnitude, while the deformation pattern is not affected and is dominated by the critical eigenmode shape (Figure 13 for K_s = 20000 and K_r = 5).

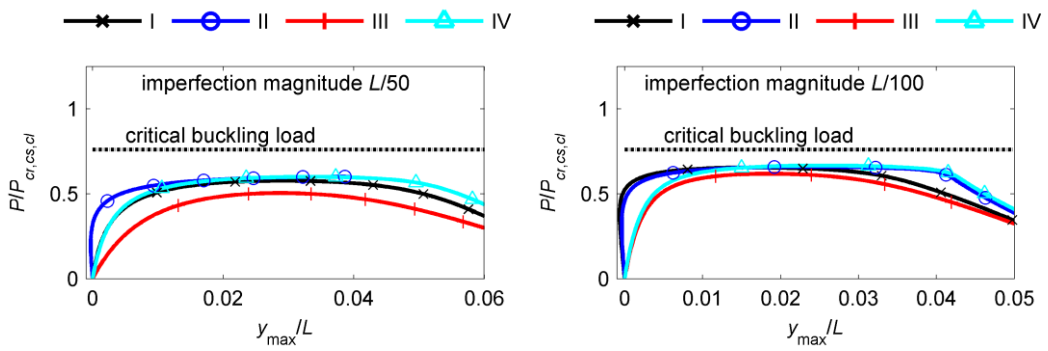

Figure 29: Equilibrium paths for varying imperfection magnitude and shape of clamped beam with two internal hinges for K_s = 20000 and rotational stiffness K_r = 5

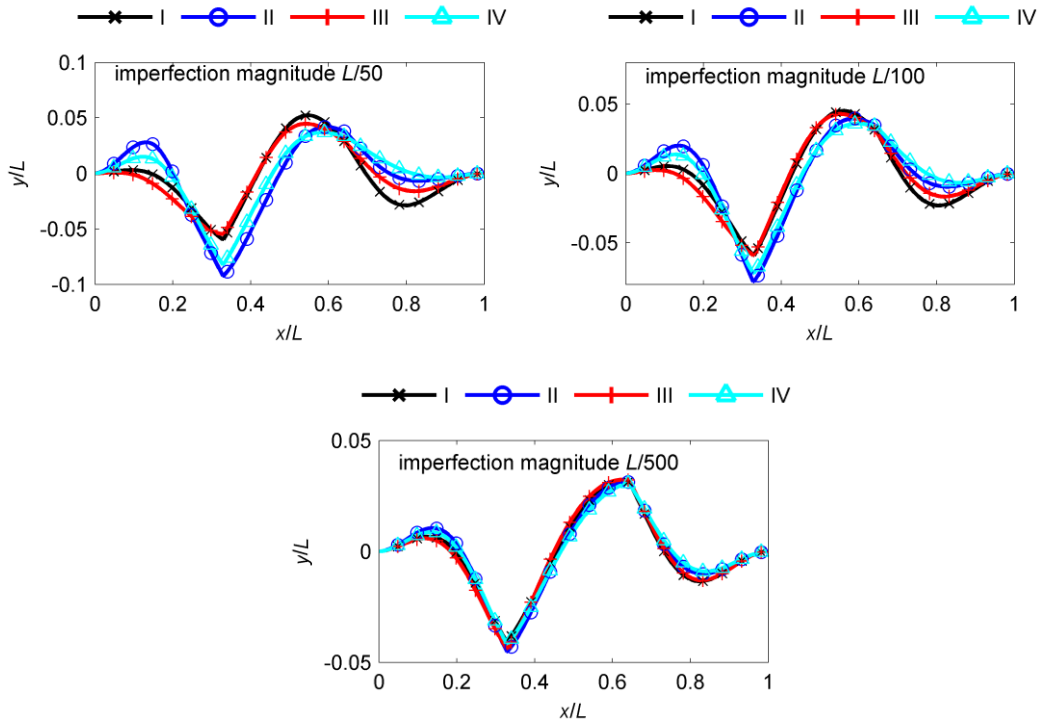

Figure 30: Equilibrium paths for varying imperfection magnitude and shape of clamped beam with two internal hinges for K_s = 20000 and rotational stiffness K_r = 5

The above results are considered as alarming for design engineers of critical structures of this type (e.g. pipelines, railway tracks) with respect to the crucial impact of the imperfection size on the structure's ultimate load, which has to be consequently taken into account in the design through proper safety factors.

4.5 EFFECT OF SOIL NONLINEARITY

Modeling soil as an elastic medium is a common and, in most cases, sufficiently reliable engineering approach to overcome the introduction of complex soil properties in numerical modeling. This approach is viable for elongated structures resting on the ground, such as railway tracks, spread footings, above ground pipelines, etc. However, buried pipelines, which are also critical elongated structures, are embedded below the ground surface, within a trench, which is then backfilled with loose granular soil. In such case the assumption of linear soil is actually far from accurate, as the overburden backfill soil has much lower stiffness than the native underlying soil. The relationship between the upward and the downward soil stiffness can be extracted from the ALA [26] provisions, or other pertinent structural codes for the design of buried pipelines against permanent ground displacements (e.g. EC8 – Part 4 [27], ASCE [28]). Thus, a reasonable estimate of the ratio of the upward soil stiffness (K_{su}) to the corresponding downward stiffness (K_{sd}) is $K_{su} / K_{sd} \approx 0.05$ (Figure 31). The effect of the different upward and downward soil stiffness is studied in the present work by considering the clamped beam with two internal hinges of Figure 4 as an appropriate structural model for buried pipelines crossing a fault. Nonlinear numerical analyses are performed by taking into account, for the sake of simplicity, only the first linear combination of eigenmodes (Table 1) as the initial geometrical imperfection shape, with magnitude $L/100$, based on the results of section 4.4 and the eigenmode shapes of the clamped beam with two internal hinges, resting on elastic soil with stiffness $K_s = 10000$, in order to carry out the comparison. The assumed hinge rotational stiffness is $K_r = 5$.

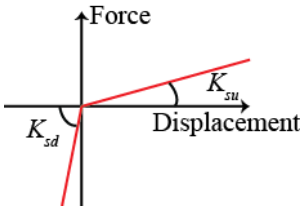

Figure 31: Relationship between upward soil stiffness (K_{su}) and the downward soil stiffness (K_{sd}) for buried pipelines

The considered soil stiffness cases are listed in Table 2, where elastic loose and elastic stiff soil are considered to exhibit K_s = 500 and K_s = 10000, respectively, while nonlinear soil exhibits different upward and downward stiffness.

Table 2: Soil stiffness for elastic and nonlinear soil properties

Soil case	K_{su}	K_{sd}
elastic loose	500	500
elastic stiff	10000	10000
nonlinear	500	10000

Numerical results in terms of the equilibrium paths are presented in Figure 32(a) indicating unstable post-buckling behavior in all cases. However, soil stiffness and soil nonlinearity highly affect the beam response. The beam behavior in case of elastic loose and of nonlinear soil is quite similar, unlike the elastic stiff case, where the beam reaches an ultimate load that is about 130% higher than the other two cases. Then, the beam deformed shapes are shown in Figure 32(b), where the beam deformation in cases of elastic soil is similar to the critical eigenmode for K_s = 10000. On the other hand, the soil nonlinearity and specifically the stiffer downward soil restricts the beam to deform downwards and consequently most of the deformation takes place upwards. The investigation outcomes of the soil nonlinearity effects highlight the necessity of considering the soil nonlinearity in the analysis and design of buried structures (e.g. pipelines), as different upward and downward soil properties reduce the ultimate load and affect the structure deformation. It is important to point out that the downward movement of a buried structure is usually highly restricted by the native soil properties. In light of this, modeling soil as an elastic medium for such structures is not on the safe side.

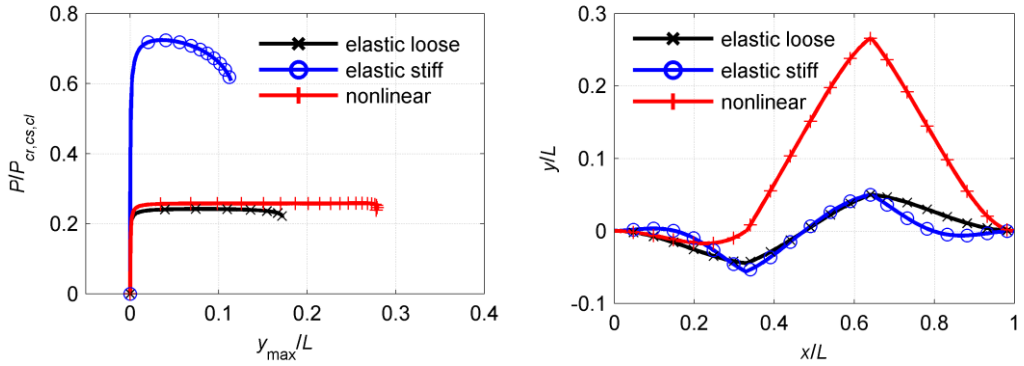

(a) (b)

Figure 32: (a) Equilibrium paths and (b) deformed shapes of clamped beam with two internal hinges with hinge rotational stiffness K_r = 5 for K_s = 10000 and considering either uniform or nonlinear soil

5. CONCLUSIONS

The buckling and post-buckling behavior of axially loaded Winkler beams internal hinges representing flexible joints has been investigated, aiming at providing a qualitative evaluation for the potential danger of upheaval buckling of buried pipelines equipped with flexible joints for their protection against failure caused by reverse fault rupture. For that purpose, a numerical approach has been selected, using the well-known and sufficiently verified commercial FEM software ADINA. This approach is considered as appropriate for dealing with the problem from a structural design rather than engineering mechanics point of view. Even though in the present investigation a straight beam model has been analyzed, supported laterally by elastic Winkler-type springs and subjected to constant axial force, the employed modeling and analysis methodology can be readily extended to issues that are commonly encountered in practice, such as non-straight pipeline route, inhomogeneous soil conditions, varying axial force distribution along the pipeline accompanied by bending moments, etc.

The beams have been analyzed as either simply-supported or clamped, having one or two internal hinges that are equipped with an elastic rotational spring, while axial and transverse displacement continuity has been assumed, modeling commercial hinged flexible joints.

Numerical linearized buckling analysis and geometrically nonlinear analysis with initial imperfections are employed to cover eigenmode cross-over and beam post-buckling behavior, particularly imperfection sensitivity, as influenced by the relation between soil stiffness and hinge rotational stiffness.

As expected, the numerical results indicate that the internal hinges reduce the beam global stiffness and thus hinged beams have lower linear and nonlinear buckling loads than continuous ones, even though this influence is substantially smaller for elastically supported beams than for laterally free ones. Increasing rotational stiffness progressively restores beam continuity. Increasing soil stiffness leads to eigenmode cross-over, provided that hinge rotational stiffness is sufficiently high. Furthermore, antisymmetric eigenmode shapes are dominated by the hinges' location on the beam, while symmetric shapes are not affected.

In nonlinear analyses, emphasis is placed on imperfection sensitivity, due to its potential significance for the ultimate buckling response. Imperfection shapes are derived from linear combinations of the first four eigenmode shapes, following common analysis practice when geometrical imperfection shapes are unknown a priori. The descending post-buckling equilibrium paths in the majority of the cases under investigation indicates that the post-buckling behavior of such internally hinged beams on Winkler foundation is unstable, with the exception of very low soil stiffness, which leads to stable post-buckling response, same as in laterally free beams. The imperfection magnitude has been found to highly influence the beam ultimate load, highlighting the need of conservative design assumptions and adoption of appropriately high safety factors. On the contrary, the imperfection shape was shown to play a relatively small role compared to imperfection magnitude for the overall buckling behavior, at least among considered imperfection shapes. Finally, considering soil to exhibit different stiffness for the upward and the downward movement, with the latter being stiffer, was found to have significant effect on the beam overall buckling response in terms of deformation shape as well as ultimate load.

The above conclusions can be useful for reevaluating the safety standards in the design against buckling of internally hinged buried pipelines subjected to reverse seismic faults. The strong dependence of the response on the relation of soil stiffness to hinge rotational stiffness, and on the size of initial imperfections, combined with the inherent uncertainties in soil properties and in excavation trench geometry, highlight the need for appropriately large safety factors.

AKNOWLEDGMENTS

This research has been co-financed by the European Union (European Social Fund – ESF) and Hellenic National Funds through the Operational Program "Education and Lifelong Learning" (NSRF 2007-2013) – Research Funding Program "Aristeia II".

REFERENCES

[1] Hetenyi H. Beams on elastic foundation: Theory with applications in the fields of civil and mechanical engineering. Ann Arbor: The University of Michigan Press; 1946

[2] Amazigo JC, Budiansky B and Carrier GF. Asymptotic analyses of the buckling of imperfect columns on non-linear elastic foundations. International Journal of Solids and Structures 1970; 6:1341-56. DOI: 10.1016/0020-7683(70)90067-3

[3] Keener JP. Buckling imperfection sensitivity of columns and spherical caps. Quarterly of Applied Mathematics 1974;34:249-56.

[4] Massalas CV, Tzivanidis GI. Equilibrium paths of a beam resting on a non-linear elastic foundation. Revue Roumaine des Sciences Techniques – Série de Mécanique Appliquée 1979; 24(2):257-62.

[5] Massalas CV, Tzivanidis GI, Katsikadelis JT. Buckling of a continuous beam resting on a tensionless elastic foundation. Journal of the Franklin Institute 1978;306(6):449-55. DOI: 10.1016/0016-0032(78)90052-2

[6] Timoshenko SP, Gere GM. Theory of elastic stability. New York: McGraw-Hill; 1961.

[7] Wu BS, Zhong HX. Postbuckling and imperfection sensitivity of fixed-end and free-end struts in elastic foundation. Archive of Applied Mechanics 1999; 69:491-8. DOI: 10.1007/s004190050237

[8] Rao GW, Neetha R. Methodology to evaluate first transition foundation stiffness for columns on Winkler foundation. ASCE Journal of Structural Engineering 2002;128:956-9. dx.doi.org/10.1061/(ASCE)0733-9445(2002)128:7(956)

[9] Kounadis AN, Mallis J, Sbarounis A. Postbuckling analysis of columns resting on an elastic foundation. Archives of Applied Mechanics 2006;75:395-404. DOI: 10.1007/s00419-005-0434-1

[10] Song X, Li SR. Thermal buckling and post-buckling of pinned-fixed Euler-Bernoulli beams on elastic foundation. Mechanics Research Communications 2007;34:164-71. DOI: 10.1016/j.mechrescom.2006.06.006

[11] Li SR, Batra RC. Thermal buckling and postbuckling of Euler-Bernoulli beams supported on nonlinear elastic foundations. American Institute of Aeronautics and Astronautics Journal 2007;45(3):712-20. DOI: 10.2514/1.24720

[12] Aristizabal-Ochoa JD. Stability of Slender columns on an elastic foundation with generalized end conditions. Ingeniería e Investigación 2013;33(3):34-40.

[13] Hunt GW, Wadee MK. Comparative Lagrangian formulations for localized buckling. Proceedings of the Royal Society A 1991;434:485-502. DOI: 10.1098/rspa.1991.0109

[14] Hunt GW, Wadee MK, Shiacolas N. Localized elasticae for the strut on the linear foundation. ASME Journal of Applied Mechanics 1993;60:1033-38

[15] Wadee MK, Hunt, Whiting AIM. Asymptotic and Rayleigh-Ritz routes to localized buckling solutions in an elastic instability problem. Proceedings of the Royal Society A 1997;453:2085-2107. DOI: 10.1098/rspa.1997.0112

[16] Hunt GW, Blackmore A. Principles of localized buckling for a strut on an elastoplastic foundation. ASME Journal of Applied Mechanics 1996;63:234-9.

[17] Melissianos VE, Vamvatsikos D, Gantes CJ. Probabilistic assessment of innovative mitigating measures for buried steel pipeline – fault crossing. Proceedings of the ASME 2015

Pressure Vessels & Piping Conference, Boston, Massachusetts, USA, 2015; Jul. 19-23. DOI: 10.1115/PVP2015-45345

[18] Melissianos VE, Gantes CJ. Earthquake induced upheaval buckling of buried pipelines with flexible joints. Second European Conference on Earthquake Engineering and Seismology, Istanbul, Turkey, 2014; Aug. 25-29.

[19] Melissianos VE, Gantes CJ. Upheaval buckling of onshore buried steel pipelines with flexible joints. Proceeding of the IASS-SLTE 2014 Symposium “Shells, Membranes and Spatial Structures: Footprints”, Brasilia, Brazil, Sept. 15-19; 2014.

[20] Wang CY. Stability of a column with two interior hinges. Mechanics Research Communications 1992;19(5):483-488. DOI: 10.1016/0093-6413(92)90030-E

[21] Wang CY. Buckling of an internally hinged column with an elastic support. Engineering Structures 2002;24:1357-1360. DOI: 10.1016/S0141-0296(02)00071-8

[22] Wang CY. Optimum location of an internal hinge of a uniform column on an elastic foundation. Journal of Applied Mechanics 2008;75(3):034501. DOI: 10.1115/1.2839635

[23] Wang CY. Buckling of a weakened infinite beam on an elastic foundation. Journal of Engineering Mechanics 2010;136(4):534-537. DOI: 10.1061/(ASCE)EM.1943-7889.0000097

[24] Dimopoulos CA, Gantes CJ. Comparison of alternative algorithms for buckling analysis of slender steel structures. Structural Engineering and Mechanics 2012;44(2):219-38.

[25] Gantes CJ, Melissianos VE. Buckling and post-buckling behavior of beams on elastic foundation modeling buried pipelines. Civil Engineering for Sustainability and Resilience International Conference, CESARE ’14, Amman, Jordan, Apr. 24-27; 2014.

[26] ALA American Lifelines Alliance. Guideline for the design of buried steel pipe – July 2001 (with addenda through February 2005). American Society of Civil Engineers, New York, USA; 2005.

[27] Comité Européen de Normalisation. Eurocode 8, Part 4: Silos, tanks and pipelines. CEN EN 1998-4, Brussels, Belgium; 2006.

[28] American Society of Civil Engineers. Guidelines for the seismic design of oil and gas pipeline systems. Committee on gas and liquid fuel life-lines, technical council on lifeline earthquake engineering, ASCE, New York, USA; 1984.

[29] O'Rourke MJ, Liu X. Seismic design of buried and offshore pipelines, Multidisciplinary Center for Earthquake Engineering Research, Buffalo; 2012.

[30] Yang G, Bradford MA. Antisymmetric post-buckling localization of an infinite column on a nonlinear foundation with softening. International Journal of Structural Stability and Dynamics 2015;15(8):1540028. DOI: 10.1142/S0219455415400283

[31] ADINA R & D Inc. Theory and Modeling guide Volume I: ADINA, Report AED 06-7, Watertown; 2006.

[32] Bathe KJ. Finite Element Procedures, Prentice-Hall, Englewood Cliffs; 1995.

[33] Brendel B, Ramm E. Linear and nonlinear stability analysis of cylindrical shells. Comput. Struct 1980;12:549-558.

[34] Nilson KF, Giannakopoulos AE. A finite element analysis of configurational stability and finite growth of buckling driven delamination. J. Mech. Phys. Solids 1995;43(12):1983-2021.

[35] Yamashita T, Kato S. Elastic buckling characteristics of two-way grid shells of single layer and its application in design to evaluate the non-linear behavior and ultimate strength. J Constr Steel Research 2001;57:1289-1308.

[36] Hoguchi H, Hisada T. Sensitivity analysis in post-buckling problems of shell structures. Computers & Structures 1993;47(4/5):699-710.

[37] Gantes CJ, Fragkopoulos KA. Strategy for numerical verification of steel structures at the ultimate limit state. Structure and Infrastructure Engineering 2010;6(1-2):225-55. DOI: 10.1080/15732470802664449

[38] Bathe KJ, Dvorkin EN. On the automatic solution of nonlinear finite element methods. Computers & Structures 1983;17(5-6):871-79.

[39] Kalochairetis KE, Gantes CJ. Experimental and numerical investigation of eccentrically loaded laced built-up steel columns. Journal of Constructional Steel Research 2014;101:66-81. DOI: 10.1016/j.jcsr.2014.04.032

[40] Zhang C, Guo Q, Zhang X. Determination of the strain-free configuration of multispan cable. Shock and Vibration 2015;article ID:890474. DOI: 10.1155/2015/890474

[41] Roy G, Braid M, Shen G. Application of ADINA and hole drilling method to residual stress determination in weldments. Computers & Structures 2003;81:929-35. DOI: 10.1016/S0045-7649(02)00478-9

[42] Yaffe R, Abramovich H. Dynamic buckling lf cylindrical stinger stiffened shells. Computers & Structures 2003;81:1031-39. DOI: 10.1016/S0045-7649(02)00417-0

[43] Yoo H, Choi D-H. New method of inelastic buckling analysis for steel frames. Journal of Constructional Steel Research 2008;64(10):1152-64. DOI: 10.1016/j.jcsr.2008.01.024

[44] Agüero A, Pallarés L, Pallarés FJ. Equivalent geometric imperfection definition in steel structures sensitive to flexural and/or torsional buckling due to compression. Engineering Structures 2015;96:160-77. DOI: 10.1016/j.engstruct.2015.03.065

[45] Schneider W, Brede A. Consistent equivalent geometric imperfection for the numerical buckling strength verification of cylindrical shells under uniform external pressure. Thin-Walled Structures 2005;43(2):175-88. DOI: 10.1016/j.tws.2004.08.006

[46] Schneider W, Timmel I, Höhn K. The conception of quasi-collapse-affine imperfections: a new approach to unfavourable imperfections of thin-walled shell structures. Thin-Walled Structures 2005;43(8):1202-24. DOI: 10.1016/j.tws.2005.03.003

NOTATION

Variables

E	elastic modulus
I	cross-section moment of inertia
x	beam longitudinal displacement
y	beam transverse displacement
L	beam length
P	compressive axial force
k_s	soil stiffness
k_r	internal hinge rotational stiffness
K_s	normalized soil stiffness
K_r	normalized hinge rotational stiffness
K_{su}	normalized upward soil stiffness
K_{sd}	normalized downward soil stiffness
P_{cr}	critical buckling load
P_u	ultimate load
P_E	Euler buckling load of continuous beam without lateral support

Subscripts

ss	simply-supported end conditions
cl	clamped end conditions
cs	continuous beam resting on foundation